LLNL-JRNL-406566

Broadband Lg Attenuation Modeling in the Middle East

M. E. Pasyanos, E. M. Matzel, W. R. Walter, A. J. Rodgers

August 26, 2008

Geophysical Journal International

This document was prepared as an account of work sponsored by an agency of the United States government. Neither the United States government nor Lawrence Livermore National Security, LLC, nor any of their employees makes any warranty, expressed or implied, or assumes any legal liability or responsibility for the accuracy, completeness, or usefulness of any information, apparatus, product, or process disclosed, or represents that its use would not infringe privately owned rights. Reference herein to any specific commercial product, process, or service by trade name, trademark, manufacturer, or otherwise does not necessarily constitute or imply its endorsement, recommendation, or favoring by the United States government or Lawrence Livermore National Security, LLC. The views and opinions of authors expressed herein do not necessarily state or reflect those of the United States government or Lawrence Livermore National Security, LLC, and shall not be used for advertising or product endorsement purposes.

Broadband Lg Attenuation Modeling in the Middle East

Michael E. Pasyanos, Eric M. Matzel, William R. Walter, Arthur J. Rodgers
Lawrence Livermore National Laboratory, Livermore, CA 94551, USA. E-mail: pasyanos1@llnl.gov

SUMMARY

We present a broadband tomographic model of Lg attenuation in the Middle East derived from source- and site-corrected amplitudes. Absolute amplitude measurements are made on hand-selected and carefully windowed seismograms for tens of stations and thousands of crustal earthquakes resulting in excellent coverage of the region. A conjugate gradient method is used to tomographically invert the amplitude dataset of over 8000 paths over a 45° x 40° region of the Middle East. We solve for Q variation, as well as site and source terms, for a wide range of frequencies ranging from 0.5 – 10 Hz. We have modified the standard attenuation tomography technique to more explicitly define the earthquake source expression in terms of the seismic moment. This facilitates the use of the model to predict the expected amplitudes of new events, an important consideration for earthquake hazard or explosion monitoring applications. The attenuation results have a strong correlation to tectonics. Shields have low attenuation, while tectonic regions have high attenuation, with the highest attenuation at 1 Hz is found in eastern Turkey. The results also compare favorably to other studies in the region made using Lg propagation efficiency, Lg/Pg amplitude ratios and two-station methods. We tomographically invert the amplitude measurements for each frequency independently. In doing so, it appears the frequency-dependence of attenuation is not compatible with the power law representation of Q(f), an assumption that is often made.

Key words: attenuation, Lg, Middle East, regional, body waves, crust, amplitudes, seismic moment

1 INTRODUCTION

Lg is a crustally guided shear-wave and is a very significant phase at regional distances over continental paths. It generally propagates at velocities ranging from 3.6 km/s to 3.1 km/s, and is recorded over a relatively wide frequency band ranging from 0.2 to 10 Hz. The amplitude of this phase, in relation to the amplitude of other regional phases such as Pn and Pg, is important in discriminating earthquakes from explosions (e.g. Kim *et al.* 1993; Walter *et al.* 1995; Hartse *et al.* 1997). The amplitude of Lg has also been used to estimate the yield of nuclear tests (e.g. Nuttli 1986; Hansen *et al.* 1990). At local distances the amplitude of shear waves is important for characterizing the earthquake hazard. For all these applications characterizing the attenuation of Lg over a wide-

frequency band is necessary in order to account for the observed large variations in amplitude.

In this paper, we present a broadband Lg attenuation model of the Middle East. The complicated tectonics of this region (**Fig. 1**) are well-known and lead to large variations in factors that affect crustally-propagating Lg such as sediment thickness, crustal velocity, and crustal thickness. Furthermore, in active tectonic regions the crustal properties can change significantly over a very small lateral ranges. As a result, we expect large attenuation variations from region to region in this area. It is therefore advantageous to make amplitude measurements for a large number of paths, so as best to cover the region with redundant data and crossing paths.

This study benefits from improvements in attenuation tomography methodology as well as improved data coverage and processing. Our methodology uses carefully measured Lg amplitudes and represents the amplitudes in several frequency bands in terms of source, path and site terms. We focused on making as many local to regional Lg single station amplitude measurements as possible for the Middle East. Our goal is to maximize the number of crossing paths and avoid the severe restrictions that exist in two-station methods. We recognize that, in addition to attenuation, observed Lg amplitudes are affected by the initial source amplitude, including corner frequency roll-off effects. In this study we explicitly formulate the source term to account for this. Additionally, the effects of geometrical spreading are removed using standard corrections. We also recognize that Lg is subject to blockage and attenuation to amplitude levels below noise levels. We use both pre-event and pre-phase signal-to-noise thresholds to remove pure noise measurements from the inversion. In fact, mapping out strong attenuation and blockage regions in the Middle East provides useful information on the geophysical structure (e.g. Kadinsky-Cade *et al.* 1981; Rodgers *et al.* 1997; Mellors *et al.* 1999; Gok *et al.* 2000; McNamara & Walter 2001; Baumgardt 2001; Sandvol *et al.* 2001). Finally, the source and geometrical spreading corrected amplitude measurements are then tomographically inverted for Q structure, as well as site and updated source terms, at a number of frequencies from 0.5 – 10 Hz. The result is a broadband attenuation model of the Middle East, which has strong correlations to the tectonic structure of the region.

We will first present the methodology used to make and correct our amplitude measurements, then review the data set, measurements, and attenuation tomography method. Next, we will discuss our results both in light of the tectonics and in comparison with other studies of the region. Finally, we will review the broad spectral attenuation at several regions in our study area, and discuss the implications of our results.

2 METHODOLOGY

In addition to along-path attenuation, the amplitude of Lg waves is controlled by the initial source, the geometrical spreading with distance, and site effects due to structure under the recording station. For a given frequency, the observed amplitude A from event i recorded at station j is a product of a source term S_i, a geometrical spreading term G_{ij}, an attenuation term B_{ij}, and a site term P_j

$$A_{ij} = S_i * G_{ij} * B_{ij} * P_j \quad (1)$$

Traditional amplitude tomographic techniques (e.g. Phillips & Stead 2008) then solve for each of the source, site and attenuation terms with tradeoffs between them. However, this results in significant source terms for each event. In addition, for explosion monitoring or earthquake hazard purposes we want to be able to apply the tomographically derived apparent attenuation to get a predicted amplitude, perhaps to use as a correction before forming a discriminant. In these cases, it would be unclear what source term is associated with the new event. Here we take a physics-based approach by explicitly defining the earthquake source in terms of the seismic moment. We begin by describing in more detail all of the terms of eq. (1), and how we will manage them in the inversion.

2.1 Geometrical spreading term

The geometrical spreading term G_{ij} is that from Street *et al.* (1975) and is given as a function of epicentral distance R:

$$G(R) = \begin{cases} 1/R & \text{if } R < R_o \\ (1/R_o)(R_o/R)^n & \text{if } R >= R_o \end{cases} \quad (2)$$

where, for Lg, n = 0.5, and the critical distance R_o is 100 km. This formula transitions from spherical spreading within the critical distance to decaying as a cylindrically spreading wave at larger distances.

2.2 Site term

The site term P_j is simply a multiplicative factor that controls the near-station amplification due to local earth structure.

2.3 Source term

The source term S_i is formulated in terms of an earthquake model tied to a measurable parameter such as the seismic moment M_o or moment magnitude M_w. Here we use the Magnitude Distance Amplitude Correction (MDAC) source model (Walter & Taylor 2001) where the earthquake source term can be expressed as a modified single corner frequency (ω_c), with ω^{-2} high frequency falloff (Aki 1967; Brune 1970):

$$S = FM_o/(1+(\omega/\omega_c))^2 \quad (3)$$

where the corner frequency ω_c is specified as:

$$\omega_c = ((K\ \sigma)/M_o)^{(1/3)} \quad (4)$$

F and K are constants that depend on medium properties, and the FM_o product is the zero-frequency spectral level. σ is the apparent stress (e.g. Wyss 1970) in the region. The source term in the tomography can be reformulated to solve for the change in moment from the assumed initial moment, where the initial value comes from a calibrated technique. In this case to predict an Lg amplitude for a new event the moment is first determined and then the 2-D Lg attenuation model and site effects are applied to get the predicted amplitude for an earthquake of that M_o and location. This is very similar to the way 1-D path corrections are commonly used to correct Lg amplitude measurements for event discrimination (e.g. Walter & Taylor 2001; Taylor *et al.* 2002) in the MDAC methodology.

The F constant is a function of the average S-wave radiation pattern $R^s_{\theta\phi}$ and the source and receiver velocities and densities and is given (Walter & Taylor 2001) by:

$$F = R^s_{\theta\phi} / 4\pi\sqrt{\rho_s \rho_r \beta_s^5 \beta_r} \qquad (5)$$

The constant *K* that governs the corner frequency ω_c used in eq. (4) is determined by the radiated energy (Walter & Taylor 2001) and is given by:

$$K = (16\pi)/(\beta_s^2 \, (R^p_{\theta\phi}{}^2 \zeta^3/\alpha_s^5)+(R^s_{\theta\phi}{}^2/ \beta_s^5)) \qquad (6)$$

where ζ is the scale factor between the P-wave and S-wave corner frequencies. The parameter values we used for the average S and P-wave radiation patterns are: $R^s_{\theta\phi}$=0.6 and $R^p_{\theta\phi}$=0.44 (Boore & Boatwright 1984). For the average source and receiver densities and velocities we used: ρ_s=2700 kg/m^3, ρ_r=2500 kg/m^3, β_s=3500 m/s, β_r=2900 m/s, and α_s= 6000 m/s. Here we use ζ=1 indicating the source P and S corner frequencies are the same.

We generalize the apparent stress in eq. (4) to the following equation

$$\sigma = \sigma' \, (M_o / M_o')^{\psi} \qquad (7)$$

For constant apparent stress, we would set ψ to 0 and σ' to the constant stress level. We have allowed the apparent stress to increase with increasing moment by specifying M_o'=1.0e15 N-m at σ' = 0.3 MPa, and use ψ = 0.25 here to match the observations of Mayeda & Walter (1996). Later in the paper, source term assumptions, such as the choice of ψ and the constancy of apparent stress, and its affect on attenuation results will be discussed in more detail.

Taylor *et al.* (2003) have previously incorporated aspects of MDAC methodology in Lg tomography in Central Asia. Several important differences exist between our methodology and that employed in their study. For example, when possible we limit ourselves to events that have seismic moment estimates rather than deriving M_o from scaling m_b. We also incorporate corner frequency differences and source-scaling changes in the radiated energy with seismic moment. As will be seen later, because of the large

number of paths, there is a significant resolution improvement from the 2° grid spacing used in Taylor *et al.* (2003). Furthermore, we also look at a frequency range spanning from 0.5 – 10 Hz, rather than a single map at 1 Hz.

2.4 Attenuation term

Lastly, the attenuation term B_{ij} is expressed in terms of Q and is given by:

$$B_{ij} = \exp[(-\omega R_{ij})/(2 Q_{ij} v)] \quad (8)$$

where R is the event-station epicentral distance, ω is the angular frequency (2πf), and v is the Lg velocity. Based on observed travel times, we use a velocity of 3.4 km/s for Lg. The Q here refers to the quality factor for the total attenuation, including both intrinsic and scattering attenuation. There is some evidence that intrinsic and scattering Q are about the same order of magnitude for Lg waves (Lacombe *et al.* 2003).

2.5 Inversion

Taking the logarithm of eq. (1), combining it with eq. (8) and correcting for geometrical spreading results in:

$$\log A_{ij} - \log G_{ij} = \log S_i + \log P_j - ((\omega \log e)/(2 Q_{ij} v)) R_{ij} \quad (9)$$

On the left-hand side the raw amplitudes are corrected for geometrical spreading. After setting initial values on the right-hand side, we solve for an updated source term (S), a site effect term (P) and the attenuation term. It is then easy to back out the values for M_o and the terms for the lateral attenuation quality factor Q.

In a recent study, Drouet *et al.* (2008) simultaneously inverted for source spectra, attenuation parameters, and site responses in southern France using data from the accelerometric network, which contains a mixture of hard and soft rock sites. While there are many similarities in the two methods, there are differences in the geometrical spreading (which does not vary with distance) and, most significantly, the Q(f) is assumed to have a power law frequency dependence, an assumption that we will be testing in our study. Furthermore, they analyze two regions where Q and its frequency dependence are solved for, but do not vary within each region. Lastly, since our study focuses on weak motion from hard rock sites, we expect smaller site corrections.

3 DATA AND TOMOGRAPHY

We have made measurements at dozens of stations in the Middle East including GSN stations (i.e. AAK, ABKT, GAR, GNI, KBL, KIV, NIL, RAYN), PASSCAL deployments (Eastern Turkey Seismic Experiment, Saudi Arabia), GEOFON stations (BGIO, CSS, EIL, ISP, MALT), MEDNET (KEG), GEOSCOPE (ATD, HYB) and stations from local networks (i.e. Saudi Arabia, Jordan, Israel, Kazakhstan, United Arab Emirates, Azerbaijan, IIEES in Iran, KOERI in Turkey). Seismicity in crust in this

region is high in particular areas. The majority of the events that we examine come from the very active Zagros Belt, although many events also originate along the Cyprean Arc, Red Sea and Gulf of Aden rifts, throughout Anatolia, along the Alborz and Kopet Dagh in Iran and in the Hindu Kush. We even have a large number of events in the mostly aseismic region of India which are aftershocks of the Bhuj earthquake. In all cases we limit the earthquakes to be within the crust (generally with depths less than 30 km).

In **Fig. 2** we show examples of waveforms in the frequency bands we examined for two different events. The top plot is a northern Iran event recorded at a station in southeast Iran. The top trace shows the unfiltered waveform, which shows the Lg phase coming in slightly faster than 3.4 km/s. The rest of the traces show the same waveform where the signal has been filtered within the frequency band listed to the right. The Lg phase records very strongly along this path between 0.5 – 4 Hz, but starts to fall off between 4 – 6 Hz and does not pass the pre-phase signal-to-noise test (explained later in this section) above 6 Hz. The bottom plot shows an event in the Gulf of Aqaba recorded at a station on the Arabian Peninsula. Here the Lg phase records well across all frequencies and dwarfs the other regional phases.

In our study, an analyst has reviewed every seismogram. If identified, the Lg arrival is picked, otherwise a theoretical arrival of 3.45 km/s is used. The phase window starts at the pick and continues to a group velocity of 2.8 km/s, with a minimum window length of 1 second. Amplitude measurements are then made in this window.

We measured Lg amplitudes for thousands of paths. For example, at 1 Hz, we have a total of 5889 paths at 53 stations from 2954 events. We tested the effect on the attenuation model of removing the paths from events recorded only at a single station. We lose significant coverage near the edge of the region, but find that the spatial variation of Q does not change over most of the coverage area. Therefore, to maximize coverage, we have included these events in our inversion.

At other frequencies, the number of paths remains high from 0.5 – 2.0 Hz, but falls to smaller numbers at higher frequencies (**Fig. 3**). At 6.0 Hz, we still have over 1000 paths, although the path coverage is not as even. **Fig. 4** shows a path map for 1 Hz showing coverage of our study area. We have excellent coverage in the central portion of the region including eastern Turkey, Iran, and the northern Arabian Peninsula. We have poorer coverage towards the periphery of our model, especially to the north and southeast where station coverage is sparse. We have no coverage of the broad oceanic region of the Arabian Sea where Lg does not propagate.

The input data consists of amplitude measurements for each path as well as moment estimates for each event. The amplitudes are time-domain RMS amplitudes converted to pseudo-spectral amplitudes (e.g. Taylor *et al.* 2002) to be compatible with the frequency domain method we are using. We only select measurements where the signal-to-noise ratio (as determined from pre-event noise) exceeds 2.0 and the signal-to-noise ratio (as determined from pre-phase noise) exceeds 1.0. This is to insure that all Lg amplitude measurements are actually from the Lg phase and not from Sn coda. The signal-to-noise

criteria, along with the lower-frequency Nyquist for some stations with lower sampling rates, are the main reasons why we have fewer paths at higher frequencies. Amplitude measurements are made in specific bands, notably 0.5-1 Hz, 1-2 Hz, 2-4 Hz, 4-6 Hz, 6-8 Hz, 8-10 Hz, and 10-12 Hz. In general, we will refer to each band by its low-frequency corner. The angular frequency used in eq. (3) and (8) is in the band range. Since the low-frequency end of the band generally has higher amplitude than the high-frequency end, the band mid-point frequency can systematically underestimate the log averaged amplitude in the band (Rodgers *et al.* 1997). We use a frequency that is ¼ of the way up the scale, so for the 1-2 Hz band, a frequency of 1.25 Hz is used.

Values of seismic moment have been estimated either using moment tensor catalogs such as the Global CMT (http://www.globalcmt.org/), regional waveform modeling or, in most cases, coda-derived estimates of this value (Mayeda *et al.* 2003). Ideally, all of our events would have such independent moment estimates. In about half of the cases, however, moments do not exist for events of interest. Therefore, where no moments are available, we have estimated a seismic moment from other magnitudes (Ms, M_L, etc.) using a regression relationship derived between the other magnitude and moments for those events where we have independent moments. The catalog magnitudes are obtained from a variety of sources (e.g. PDE, ISC, regional networks) and vary somewhat in methods and estimated magnitudes.

Referring back to eq. (9), we correct the amplitudes for geometrical spreading and solve for lateral Q, the source terms S_i, and the site terms P_j. The region is parameterized into a grid of equal area cells. At frequencies of 0.5-4 Hz, we use 0.5° cells, while for higher frequencies we have fewer paths and use 0.75° cells. A single attenuation value is used as the starting model, which follows a power law model:

$$Q(f) = Q_o f^{\eta} \qquad (10)$$

where Q_o = 275 and η = 0.725. During the inversion each frequency is solved for independently and, while the model quickly moves away from the starting model where there is data, the starting model persists in regions without any paths. The source terms are then converted to seismic moment or moment magnitude through the source term equations. We also solve for site terms at every station for each frequency band, which is representative of the local station site effects. A Laplacian function is used to smooth the variation in Q between adjacent cells and to regularize the tomography. A conjugate gradient method is used as the solver.

For many reasons (e.g. focusing/defocusing, multi-pathing, blockage, source complications, etc.), seismic amplitude residual data is highly variable, much more so than seismic velocities. After the inversion, the RMS error is reduced from a misfit of 0.60 log-units (~4.0) with the starting model (single Q, no site effects, initial source terms) to about 0.15 log-units (~1.4) (**Fig. 5**). This is a variance reduction of about 94%. Note that it is possible to fit the data to an even higher level by eliminating the smoothing and/or putting more of the amplitude variations into site and event corrections. This,

however, is simply a function of overfitting the data with significantly more degrees of freedom.

4 RESULTS

The attenuation of 1 Hz Lg is shown by the map in **Fig. 6**. In each of the attenuation plots, warm colors represent low Q (high attenuation) and cool colors represent high Q (low attenuation). Note that Q is plotted on a logarithmic scale with values annotated every 0.25 in $\log_{10}$ space.

The results show a significant variation in the Q values. Attenuation is very high in the Turkish-Iranian Plateau (Q < 200), high along the Zagros Mts. and portions of the Red Sea and Gulf of Aden rifts (Q = 200-300), moderate in the northern Arabian Plate (Q = 300-400), low in the Arabian Platform and Kazakh Platform (Q = 400-600), and very low in the Arabian Shield and Indian Shield (Q > 800). The lowest Q is found in eastern Turkey (Q=150) and the highest is found in the Indian Shield (Q ~ 2000). While the results are very complicated, there appear to be significant correlations between Q values and age of most-recent tectonic activity, with areas of recent activity having low Q and areas of older thermo-tectonic events having high Q.

One correlation (comparing **Figs 1 and 6**, for example) is the relationship between topography and crustal attenuation. It appears that large topography variations, both high topography in mountain ranges and low topography in extended regions, are a surrogate for crustal deformation. Tectonically-affected regions with significant crustal deformation have lower Q (higher attenuation) than undeformed regions. Another observation is that features that we would expect to produce large effects in the mantle (e.g. uplift of the Turkish and Iranian Plateaus) seem to also have large effects on Lg attenuation. This could be an effect of lithospheric thickness and heat flow on the crustal attenuation. Studies of Lg propagation have sought deterministic relationships between Lg amplitudes or amplitude ratios and path-specific crustal waveguide properties (e.g. Zhang & Lay 1994; Fan & Lay 1998; Rodgers *et al.* 1999). These generally studies report weaker Lg amplitudes (higher Pn/Lg or Pg/Lg ratios) for paths crossing high and/or rough topography.

In the inversion, a site amplification term is solved for at each station. Values of the site terms range from as low as 0.15 to as high as about 3.4 (for HYB). **Fig. 7** shows a map of site terms. Unlike the attenuation maps, the site terms don't appear to correlate well with seismic structure, which is probably expected if the site terms reflect local effects. We also performed a test where one station had the wrong gain, and found that it was directly absorbed into the site factor and had no impact on the attenuation maps.

The inversion also solves for source terms (which can be characterized as M_w corrections) for each event. In general, changes to the event terms (shown in **Fig. 8**) are relatively small. Except for a few rare cases (which are probably poor magnitude estimates), the largest M_w differences are 0.3-0.4 magnitude units and the overall average (RMS) difference is only ~0.2 magnitude units. When we break it down by magnitude

type, however, we find that the RMS differences between the original and new M_w is ~0.23 m.u. for converted magnitudes and only 0.17 m.u. for true moments. This supports our supposition that, when available, independent rather than magnitude regression derived moments should be used. It also demonstrates that the method is able to compensate for bad initial M_ws, rather than biasing the spatial attenuation. Small M_w corrections are found across the frequency band except at 8.0 Hz where there are fewer paths and more events with amplitudes recorded at only a single station.

We compare our results to several other 1 Hz Lg Q models of the Middle East, those of Sandvol *et al.* (2001), Al-Damegh *et al.* (2004), and Zor *et al.* (2007), and one for the Indian Platform (Mitra *et al.* 2006).

Sandvol *et al.* (2001) estimated Lg/Pg relative attenuation by applying tomography to 4400 Lg/Pg amplitude ratios. Al-Damegh *et al.* (2004) added more data (for a total of 6200 paths) and improved the Lg/Pg efficiency maps. Because it is a relative attenuation method, these studies do not obtain values of Lg Q. However, they find efficient Lg propagation within the Arabian Plate and some parts of the Red Sea and inefficient or blocked propagation in the Zagros and Turkish-Iranian Plateau. In general, this is consistent with the results that we find here, although there are differences in the Makran region of southeast Iran and southwest Pakistan.

Zor *et al.* (2007) used a two-station method to measure interstation Lg Q along 296 unblocked paths and 154 blocked paths. They then invert the measurements to obtain Q_o and η models of a much smaller than the region we consider in this study. The results are more or less similar to the qualitative methods discussed above. They find low to normal Q_o values (250-350) in the northern Arabian Platform, high Q_o values (670-800) in the southern Arabian Plate, very low Q_o in the Turkish Plateau (100-200). The lowest Q_o values are found in the East Anatolian Plateau (70-100). The authors also find a negative correlation between Q_o and η. In general, the Q values that they obtain are quite similar to those we find here.

Mitra *et al.* (2006) used the decay of spectral amplitudes with distance from 3 events to determine average Lg attenuation in the Indian Platform. While their average values for the region $Q = 655(\pm 10)\ f^{0.67(\pm 0.03)}$ are lower than the values that we found for the Indian Shield ($Q > 800$), they are more consistent with the higher values that they found for paths emanating from the shield - $Q = 869(\pm 45)\ f^{0.64(\pm 0.11)}$.

Except as noted (e.g. grid size) we follow the same procedures for all other frequencies in our analysis. Results are shown in **Fig. 9**. Ranges of Q values are recorded in **Table 1**. Some maps of Lg attenuation for different frequencies are quite similar, particularly those going from 0.5 Hz to 1.0 Hz to 2.0 Hz. In these three plots, the relative variations are generally similar, but the absolute Q values increases with frequency. This pattern seems to break down at higher frequencies, although there are several features in the 4.0 Hz map (eastern Turkey, Red Sea, central Iran) that seem persistent. Maps at higher frequencies are quite dissimilar, likely because the number of paths has fallen off rather significantly (**Fig. 3**).

With the set of inversions for several frequency bands, it is easy to produce average frequency-dependent Q plots for any particular region. In **Fig. 10**, we assemble and compare of Q(f) for 4 well-covered regions of interest within our study area: the Central Zagros, the Northern Arabian Platform, Indian Shield, and Eastern Turkey. First, it appears that Eastern Turkey has the highest attenuation over the whole band. The Central Zagros is also a high attenuation region at low frequency, but has high Q at high frequencies. The Northern Arabian Platform has low attenuation at the low frequency end, but has moderate attenuation at high frequencies, while the Indian Shield has low attenuation across all frequencies. In all cases, however, we find that Q(f) is not well represented by the power law (as represented by our starting model in eq. (10)), which is often assumed in many studies (e.g. Mitchell *et al.* 1997; Erickson *et al.* 2004; Mitra *et al.* 2006; Zor *et al.* 2007). We note that this divergence from the power law does not occur only at high-frequencies, where we have less confidence in the tomographic maps, but also at the lower-frequency end, where the inversion results are well-resolved.

One source parameter in the inversion that is not independently well constrained is the apparent stress. We experimented with both a constant apparent stress and an apparent stress that increases with moment as some recent studies have found (e.g. Mayeda & Walter 1996, Mayeda *et al.* 2007). We ran the models both for the case of $\psi = 0$ and $\psi = 0.25$. The change in the attenuation maps between the two cases was negligible (RMS difference in log Q of 0.04), indicating that the attenuation maps are robustly determined for a range of source parameters. The source correction terms changed more significantly between the two cases. For the constant apparent stress case the source corrections at 1 Hz showed a less linear and stronger variation with moment than the case of ψ=0.25, particularly for the largest events where there was large misfit between the original moment estimates (generally events having CMT solutions) and the new estimates. For this reason we prefer the ψ=0.25 case and that is what is shown in **Fig. 8**.

5 CONCLUSIONS

We have developed a broadband Lg attenuation model of the Middle East. We make single station absolute amplitude measurements and use a model-based formalism, which provides better path coverage and higher resolution than relative two-station measures. The amplitude measurements are then corrected for magnitude and distance effects in order to isolate the path attenuation. Tomographic inversion of the data produces models that are consistent with the complex tectonics of the region. In particular, there appear to be strong correlations with both topography and tectonic character. They are also consistent with models derived from two-station measurements. In addition, we are able to derive attenuation models over a wide frequency band (0.5 – 10 Hz) allowing us to examine frequency-dependent Q in the region. We conclude that power law Q (as represented by Q_o and η) is not a good way of capturing the Q variation over this frequency range.

The estimated region-specific Lg Q model developed in this study can be used to constrain ground motion predictions for seismic hazard assessment. The wide range of

inferred Q values would indicate that strong ground motions for a given event would attenuate much more slowly in regions of high Q and should be factored into probabilistic seismic hazard assessment in the Middle East.

Besides improving our attenuation models with more data, particularly at the highest frequencies, in the future we would like to investigate the possibility of inverting our frequency-dependent $Q_{Lg}(f)$ models for depth-dependent $Q_s(z)$ models. This will require more measurements and better tomographic maps at the highest frequencies, where the path coverage is poorest. This is complicated by several factors. The first is the fact that some of the stations considered have lower sampling rates. The second factor is that, even with higher Q, amplitude falloff is more pronounced at higher frequencies due to the larger number of cycles. This requires larger events and shorter paths to make quality measurements.

ACKNOWLEDGMENTS

This work would not have been possible without the dedicated programming efforts of Doug Dodge and Mike Ganzberger on the Regional Body-wave Amplitude Processing (RBAP) program. We thank Terri Hauk for loading the data into the LLNL research database and Stan Ruppert for setting up and maintaining the LLNL computational infrastructure. We thank Flori Ryall for the many regional phase picks used in this study. We are also thankful to all of the agencies that have contributed data for this work. Most figures were prepared using GMT [Wessel & Smith 1998]. This work was performed under the auspices of the U.S. Department of Energy by Lawrence Livermore National Laboratory under Contract DE-AC52-07NA27344. This is LLNL contribution LLNL-JOUR-??????.

REFERENCES

Aki, K., 1967. Scaling law of seismic spectrum, *J. Geophys. Res.*, **72,** 729-740.

Al-Damegh, K., Sandvol, E., Al-Lazki, A. & Barazangi, M., 2004. Regional seismic wave propagation (Lg and Sn) and Pn attenuation in the Arabian Plate and surrounding regions, *Geophys. J. Int.*, **157,** 775-795, doi:10.1111/j.1365-246X.2004.02246.x.

Baumgardt, D., 2001. Sedimentary basins and the blockage of Lg wave propagation in the continents, *Pure appl. Geophys.*, **158,** 1207-1250.

Boore, D.M. & Boatwright, J., 1984. Average body-wave radiation coefficients, *Bull. Seism. Soc. Amer.*, **74,** 1615-1621.

Brune, J., 1970. Tectonic stress and the spectra from seismic shear waves earthquakes, *J. Geophys. Res.*, **75,** 4997-5009.

Drouet, S., Chevrot, S., Cotton, F. & Souriau, A., 2008. Simultaneous inversion of source spectra, attenuation parameters, and site responses: Application to the data of the French accelerometric network, *Bull. Seism. Soc. Amer.*, **98,** 198-219, doi:10.1785/0120060215.

Erickson, D., McNamara, D.E. & Benz, H.M., 2004. Frequency-dependent Lg Q within the continental United States, *Bull. Seism. Soc. Amer.*, **94,** 1630-1643.

Fan, G. & Lay, T., 1998. Statistical analysis of irregular waveguide influences on regional seismic discriminants in China, *Bull. Seism. Soc. Am.*, **88**, 74-88.

Gok, R., Turkelli, N., Sandvol, E., Seber, D. & Barazangi, M., 2000. Regional wave propagation in Turkey and surrounding regions, *Geophys. Res. Lett.*, **27,** 429-432.

Hansen, R.A., Ringdal, F. & Richards, P.G., 1990. The stability of rms Lg measurements and their potential for accurate estimation of the yields of Soviet underground nuclear explosions. *Bull. Seism. Soc. Amer.*, **80,** 2106-2126.

Hartse, H.E., Taylor, S.R., Phillips, W.S. & Randall, G.E., 1997. A preliminary study of regional seismic discrimination in central Asia with emphasis on western China, *Bull. Seism. Soc. Amer.*, **87,** 551-568.

Kadinsky-Cade, K., Barazangi, M., Oliver, J. & Isacks, B., 1981. Lateral variations of high-frequency seismic wave propagation at regional distances across the Turkish and Iranian plateaus, *J. Geophys. Res.*, **86,** 9377-9396.

Kim, W.-Y., Simpson, D. & Richards, P., 1993. Discrimination of earthquakes and explosions in the eastern United States using regional high-frequency data, *Geophys. Res. Lett.*, **20,** 1507-1510.

Lacombe, C., Campillo, M., Paul, A. & Margerin, L., 2003. Separation of intrinsic absorption and scattering attenuation from Lg coda decay in central France using acoustic radiative transfer theory, *Geophys. J. Int.,* **154**, 417-425, doi: 10.1046/j.1365-246X.2003.01976.x

Mayeda, K. & Walter, W.R., 1996. Moment, energy, stress drop, and source spectra of western U.S. earthquakes, *J. Geophys. Res.*, **101,** 11195-11208.

Mayeda, K., Hofstetter, A., O'Boyle, J.L. & Walter, W.R., 2003. Stable and transportable regional magnitudes based on coda-derived moment-rate spectra, *Bull. Seism. Soc. Amer.*, **93,** 224-239.

Mayeda, K., Malagnini, L. & Walter, W.R., 2007. A new spectral ratio method using narrow band coda envelopes: Evidence for non-self-similarity in the Hector Mine sequence, *Geophys. Res. Lett.*, **34,** L11303, doi:10.1029/2007GL030041, 2007.

McNamara, D. & Walter, W., 2001. Mapping crustal heterogeneity using Lg propagation efficiency throughout the Middle East, Mediterranean, southern Europe and northern Africa, *Pure appl. Geophys.*, **158,** 1165-1188.

Mellors, R., Vernon, F., Camp, V., Al-Amri, A.M. & Gharib, A., 1999. Regional waveform propagation in the Saudi Arabian Peninsula and evidence for a hot upper mantle under western Arabia, *J. Geophys. Res.*, **104,** 20,221-20,235.

Mitchell, B.J., Pan, Y., Xie, J. & Cong, L., 1997. Lg coda Q variation across Eurasia and its relation to crustal evolution, *J. Geophys. Res.*, **102,** 22,767–22,779.

Mitra, S., Priestley, K., Gaur, V.K. & Rai, S.S., 2006. Frequency-dependent Lg attenuation in the Indian Platform, *Bull. Seism. Soc. Amer.*, **96,** 2449-2456, doi:10.1785/0120050152.

Nuttli, O.W., 1986, Yield estates of Nevada Test Site explosions obtained from seismic Lg waves, *Bull. Seism. Soc. Amer.*, **91,** 2137-2151.

Phillips, W.S. & Stead, R.J., 2008. Attenuation of Lg in the western U.S. using the USArray, *Geophys. Res. Lett.*, **35,** L07307, doi:10.1029/2007GL032926.

Rodgers, A., Ni, J. & Hearn, T., 1997. Propagation characteristics of short-period Sn and Lg in the Middle East, *Bull. Seism. Soc. Amer.*, **87,** 396-413.

Rodgers, A.J., Lay, T., Walter, W.R. & Mayeda, K., 1997. A comparison of regional-phase amplitude ratio measurement techniques, *Bull. Seism. Soc. Amer.*, **87,** 1613-1621.

Rodgers, A.J., Walter, W.R., Schultz, C.A., Myers, S.C. & Lay, T., 1999. A comparison of methodologies for representing path effects on regional P/S discriminants, *Bull. Seism. Soc. Am.*, **89,** 394-408.

Rodgers, A. & Walter, W., 2002. Seismic discrimination of the May 11, 1998 Indian nuclear test with short-period regional data from station NIL (Nilore, Pakistan), *Pure appl. Geophys.*, **159,** 679-700.

Sandvol, E., Al-Damegh, K., Calvert, A., Seber, D., Barazangi, M., Mohamed, R., Gok, R., Turkelli, N. & Gurbuz, C., 2001. Tomographic imaging of Lg and Sn propagation in the Middle East, *Pure appl. Geophys.*, **158,** 1121-1163.

Street, R.L., Herrmann, R. & Nuttli, O., 1975. Spectral characteristics of the Lg wave generated by central United States earthquakes, *Geophys. J. R. Astron. Soc.*, **41,** 51-63.

Taylor, S.R., Velasco, A.A., Hartse, H.E., Phillips, W.S., Walter, W.R. & Rodgers, A.J., 2002. Amplitude corrections for regional seismic discriminants, *Pure appl. Geophys.*, **159,** 623-650.

Taylor, S.R., Yang, X. & Phillips, W.S., 2003. Bayesian Lg attenuation tomography applied to Eastern Asia, *Bull. Seism. Soc. Amer.*, **93,** 795-803.

Walter, W.R., Mayeda, K.M. & H.J. Patton, 1995. Phase and spectral ratio discrimination between NTS earthquakes and explosions. Part I: Empirical observations, *Bull. Seism. Soc. Amer.*, **85,** 1050-1067.

Walter, W.R. & Taylor, S.R., 2001. A revised magnitude and distance amplitude correction (MDAC2) procedure for regional seismic discriminants: theory and testing and NTS, Lawrence Livermore National Laboratory, UCRL-ID-146882 http://www.llnl.gov/tid/lof/documents/pdf/240563.pdf

Wessel, P. & Smith, W.H.F., 1998. New, improved version of Generic Mapping Tools released, *EOS trans. AGU,* **79,** 579.

Wyss, M., 1970, Stress estimates of South American shallow and deep earthquakes, *J. Geophys. Res.*, **75,** 1529-1544.

Zhang, T. & Lay, T., 1994. Analysis of short-period regional phase path effects associated with topography in Eurasia, *Bull. Seism. Soc. Am.,* **84**, 119-132.

Zor, E., Sandvol, E., Xie, J., Türkelli, N., Mitchell, B., Gasanov, A.H. & Yetirmishli, G., 2007. Crustal attenuation within the Turkish Plateau and surrounding regions, *Bull. Seism. Soc. Amer.*, **97,** 151-161.

Table 1. Q ranges in each frequency band.

Frequency (Hz)	Log Q ± s.d.	Mean	Mean ± 2*s.d.
0.5	2.32 ± 0.19	208	84 – 511
1.0	2.50 ± 0.16	321	150 – 678
2.0	2.73 ± 0.15	541	271 – 1066
4.0	2.97 ± 0.24	951	317 – 2852
6.0	3.12 ± 0.29	1315	348 – 4975
8.0	3.18 ± 0.21	1512	567 – 4027

Figure captions

Figure 1. Topographic map of the Middle East study area showing place names and tectonic regions referenced in the text. The thick black lines indicate plate boundaries. White crosses are the locations of further analysis later in the paper.

Figure 2. a) An event in Northern Iran recorded at station ZHSF in southeast Iran. The top trace shows the unfiltered waveform over the same trace plotted in a filter comb from 0.5 – 10 Hz. b) An event in the Gulf of Aqaba recorded at station AFIF in central Arabia.

Figure 3. Number of Lg paths passing the signal-to-noise criteria as a function of frequency.

Figure 4. Path map of Lg attenuation measurements in the Middle East. Stations are shown by yellow triangles, events by green circles, and paths by blue lines.

Figure 5. Histograms of log10 amplitude residuals at 1.0 Hz for the initial model (top) and after the inversion (bottom). The y-axis shows the frequency-percentage in percent.

Figure 6. Attenuation map of Lg Q at 1 Hz in the Middle East. Q values range from under 200 to over 1000. Note that the Q scale is logarithmic.

Figure 7. Plot showing site amplification terms solved for at 1 Hz. Values range from 0.15-3.4. A value of 1.0 indicates normal site term values.

Figure 8. Plot showing event terms (represented as moment magnitude) solved for at 1 Hz. Values on the x-axis are M_w values derived from the original moments, and values on the y-axis are the new M_w values. Symbols indicate if the original M_ws were either magnitude-derived (triangles) or true seismic moments (circles).

Figure 9. Attenuation maps of Lg Q at frequencies of 0.5 Hz, 1 Hz, 2 Hz, 4 Hz, 6 Hz, and 8 Hz. Note that the Q-scale varies from figure to figure in order to capture the variations in this parameter.

Figure 10. Plot of frequency-dependent attenuation for four selected regions in our study area: Central Zagros (black), North Arabian Platform (red), Indian Shield (green), and Eastern Turkey (blue). The dashed line shows the power-law starting model.

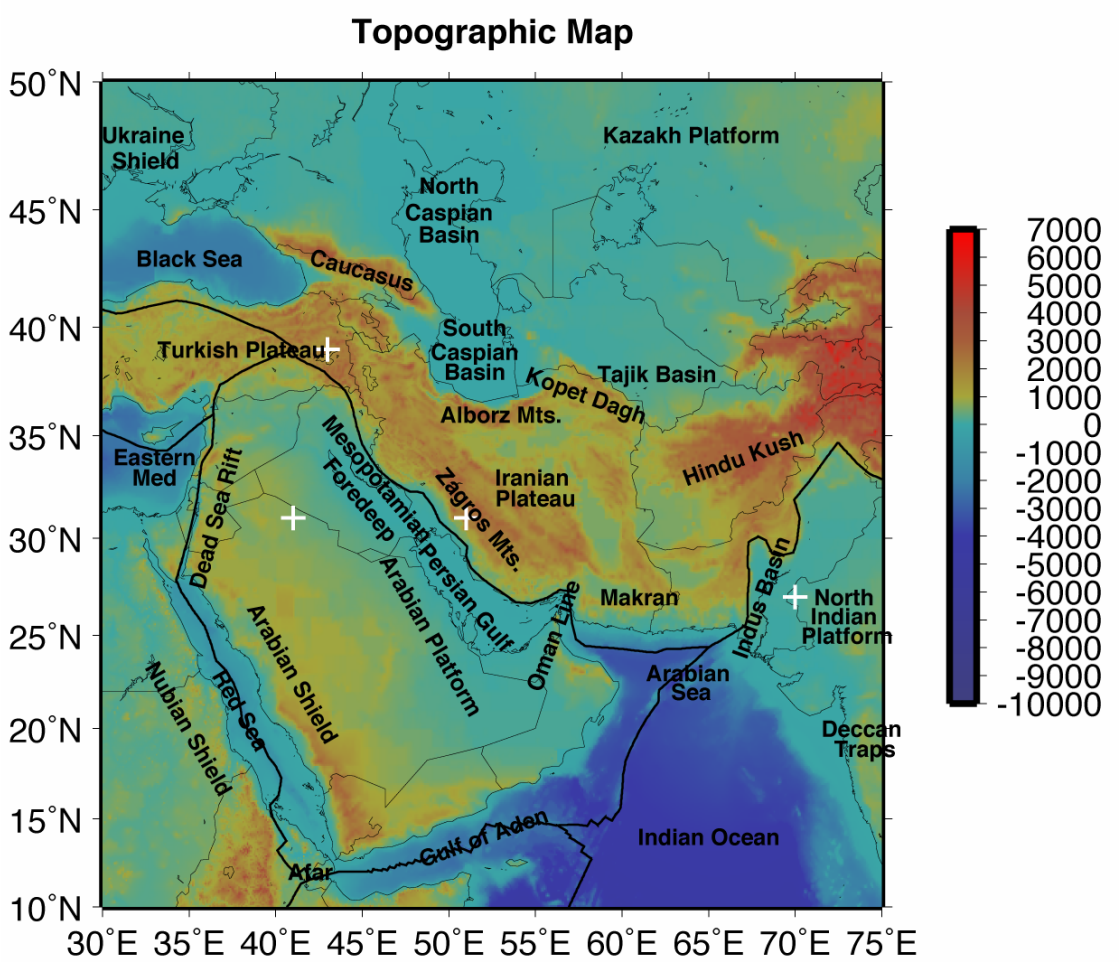
Topographic Map
50°N
45°N
40°N
35°N
30°N
25°N
20°N
15°N
10°N
30°E 35°E 40°E 45°E 50°E 55°E 60°E 65°E 70°E 75°E
Ukraine Shield
Kazakh Platform
North Caspian Basin
Black Sea
Caucasus
Turkish Plateau
South Caspian Basin
Tajik Basin
Kopet Dagh
Alborz Mts.
Eastern Med
Dead Sea Rift
Mesopotamian Foredeep
Zagros Mts.
Iranian Plateau
Hindu Kush
Arabian Platform
Persian Gulf
Oman Line
Makran
Indus Basin
North Indian Platform
Arabian Shield
Red Sea
Nubian Shield
Arabian Sea
Deccan Traps
Gulf of Aden
Afar
Indian Ocean
7000
6000
5000
4000
3000
2000
1000
0
-1000
-2000
-3000
-4000
-5000
-6000
-7000
-8000
-9000
-10000

Figure 1

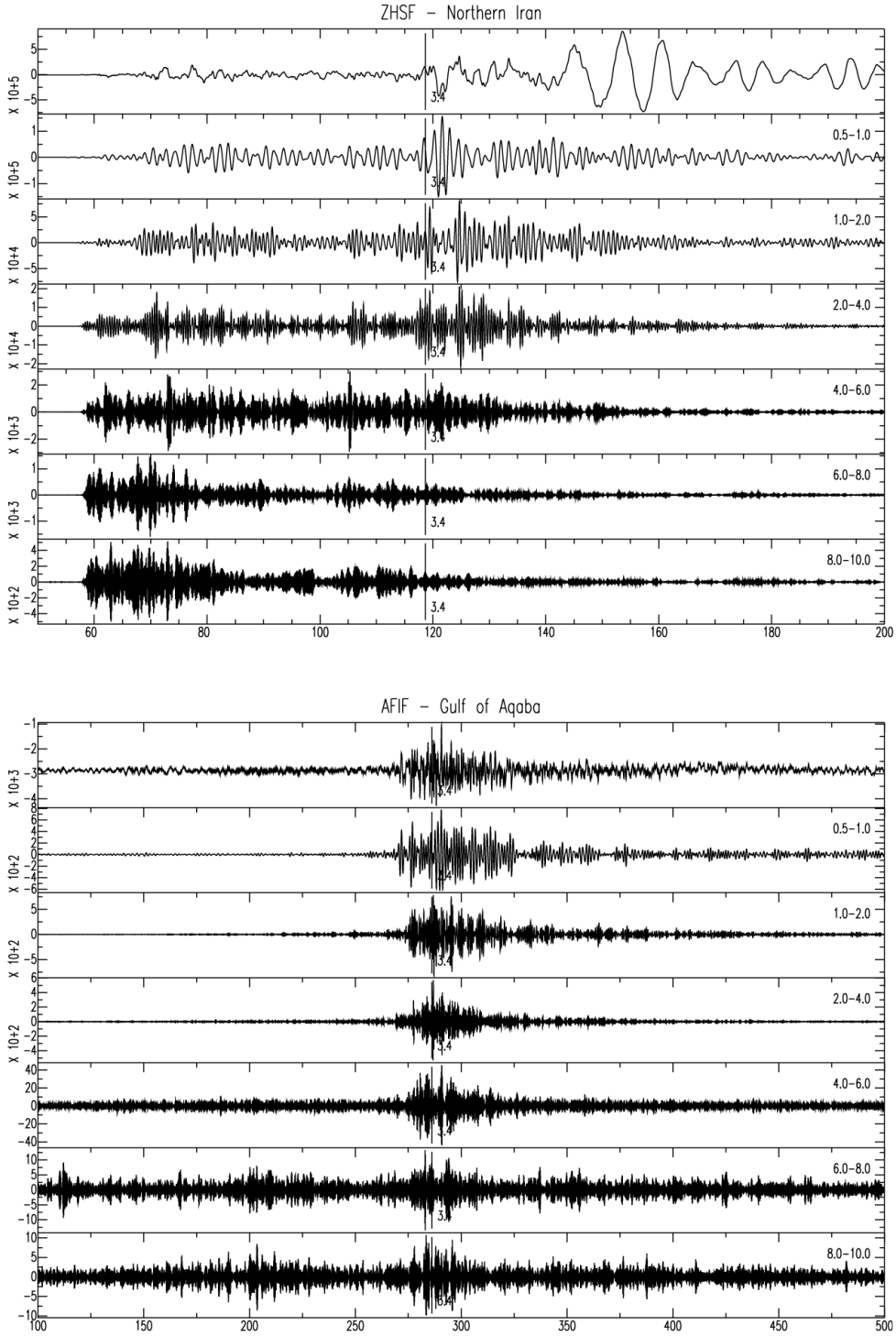
ZHSF – Northern Iran
0.5–1.0
1.0–2.0
2.0–4.0
4.0–6.0
6.0–8.0
8.0–10.0
X 10+5
X 10+4
X 10+3
X 10+2
3.4
AFIF – Gulf of Aqaba

Figure 2

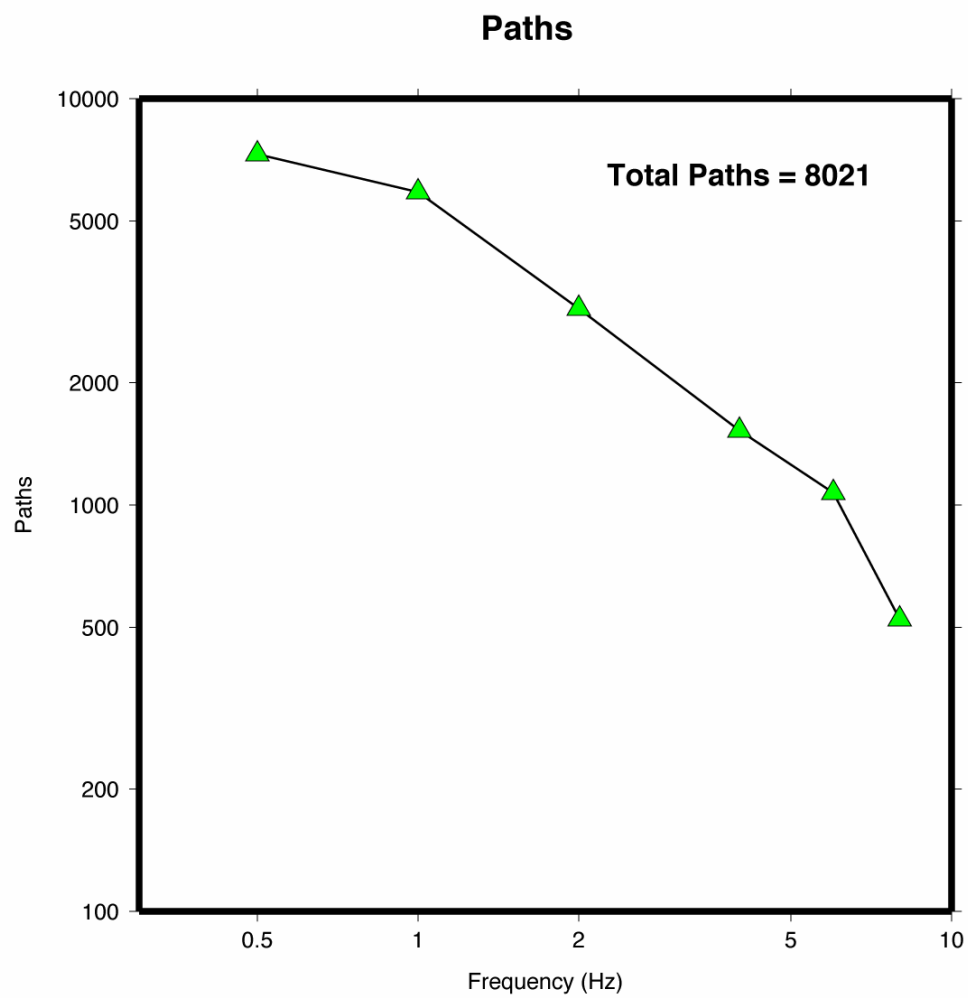
Paths
Total Paths = 8021
10000
5000
2000
1000
500
200
100
Paths
0.5
1
2
5
10
Frequency (Hz)

Figure 3

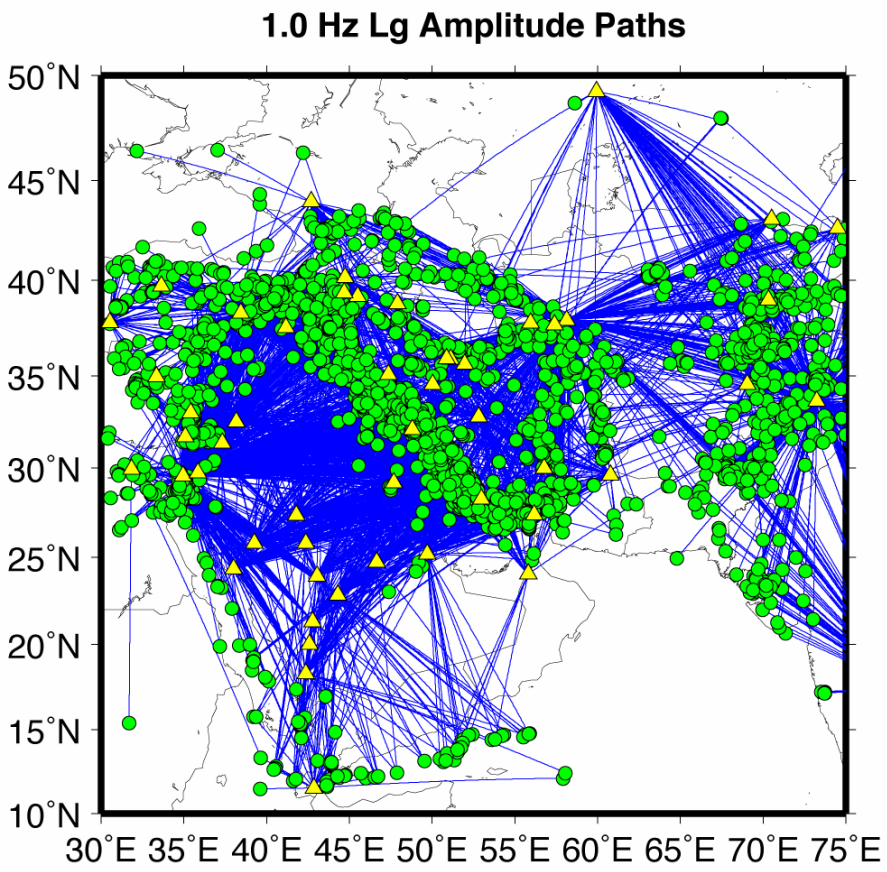
1.0 Hz Lg Amplitude Paths
50˚N
45˚N
40˚N
35˚N
30˚N
25˚N
20˚N
15˚N
10˚N
30˚E 35˚E 40˚E 45˚E 50˚E 55˚E 60˚E 65˚E 70˚E 75˚E

Figure 4

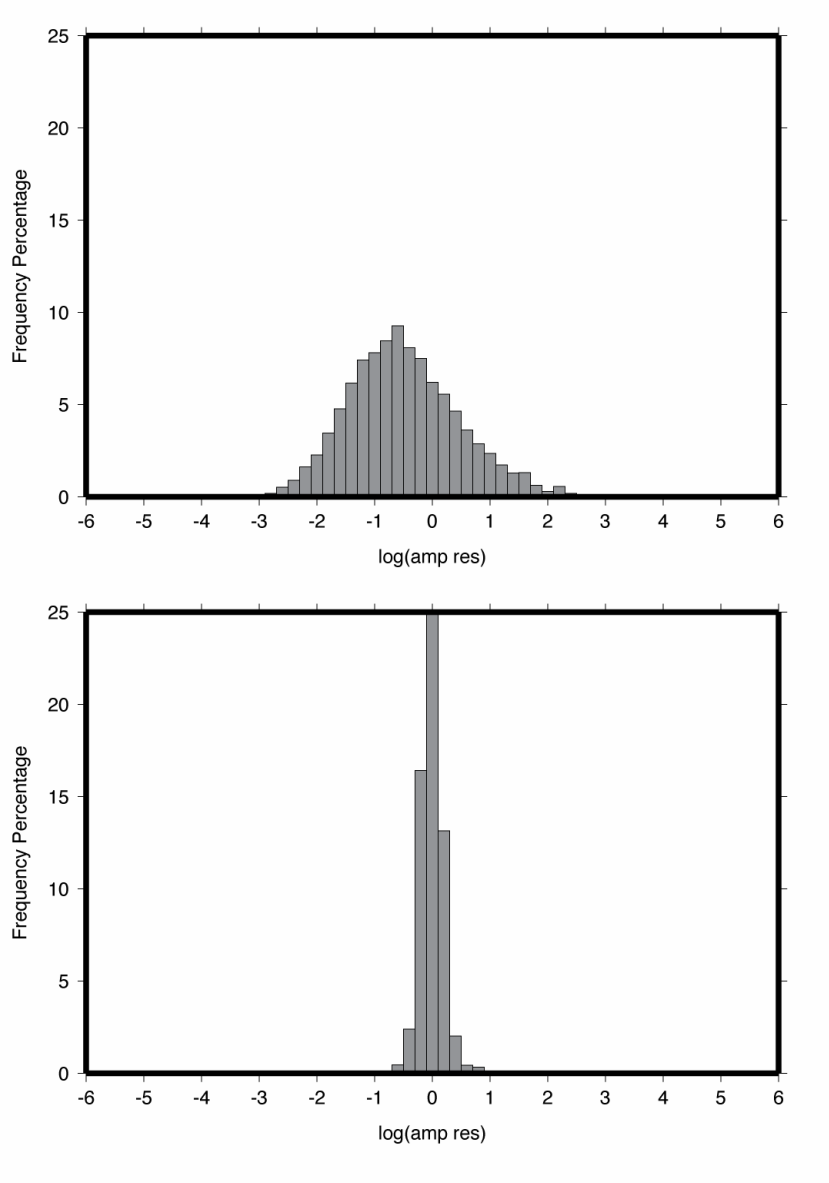
Frequency Percentage
log(amp res)
Frequency Percentage
log(amp res)

Figure 5

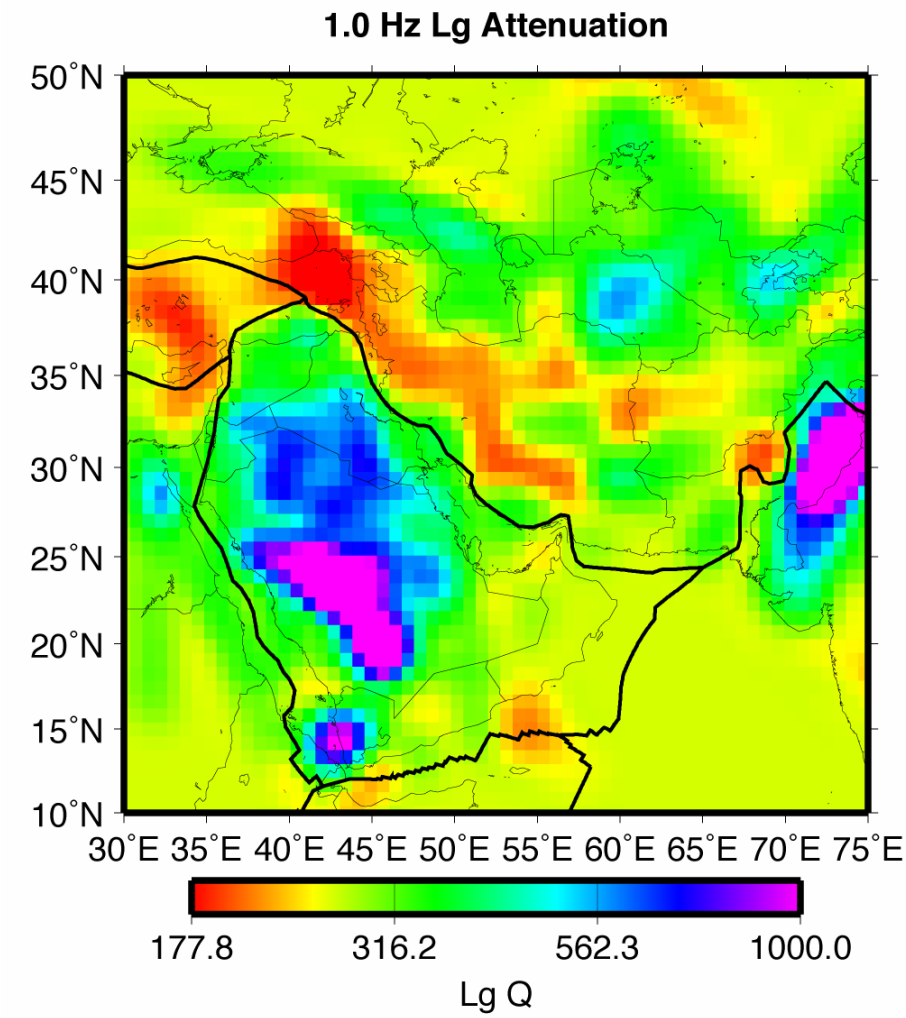
1.0 Hz Lg Attenuation
50˚N
45˚N
40˚N
35˚N
30˚N
25˚N
20˚N
15˚N
10˚N
30˚E 35˚E 40˚E 45˚E 50˚E 55˚E 60˚E 65˚E 70˚E 75˚E
177.8
316.2
562.3
1000.0
Lg Q

Figure 6

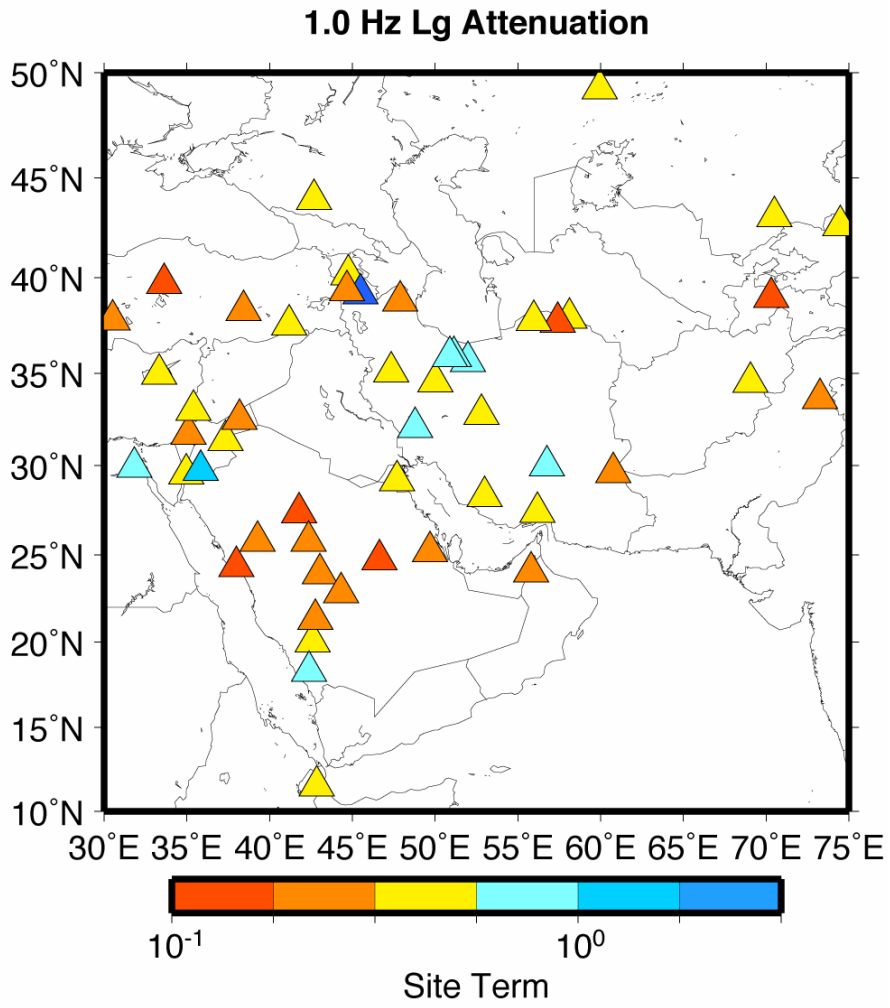
1.0 Hz Lg Attenuation
50˚N
45˚N
40˚N
35˚N
30˚N
25˚N
20˚N
15˚N
10˚N
30˚E 35˚E 40˚E 45˚E 50˚E 55˚E 60˚E 65˚E 70˚E 75˚E
10-1
100
Site Term

Figure 7

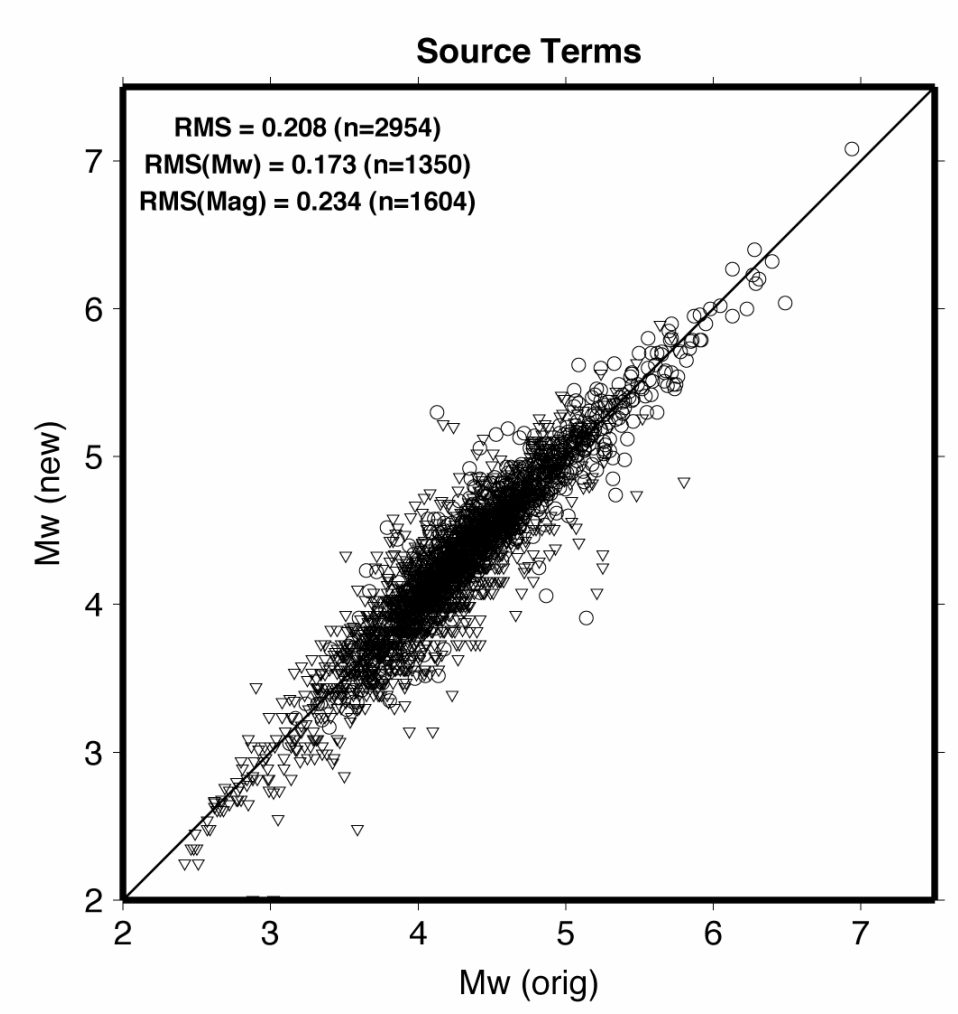
Source Terms
RMS = 0.208 (n=2954)
RMS(Mw) = 0.173 (n=1350)
RMS(Mag) = 0.234 (n=1604)
Mw (new)
Mw (orig)
2
3
4
5
6
7

Figure 8

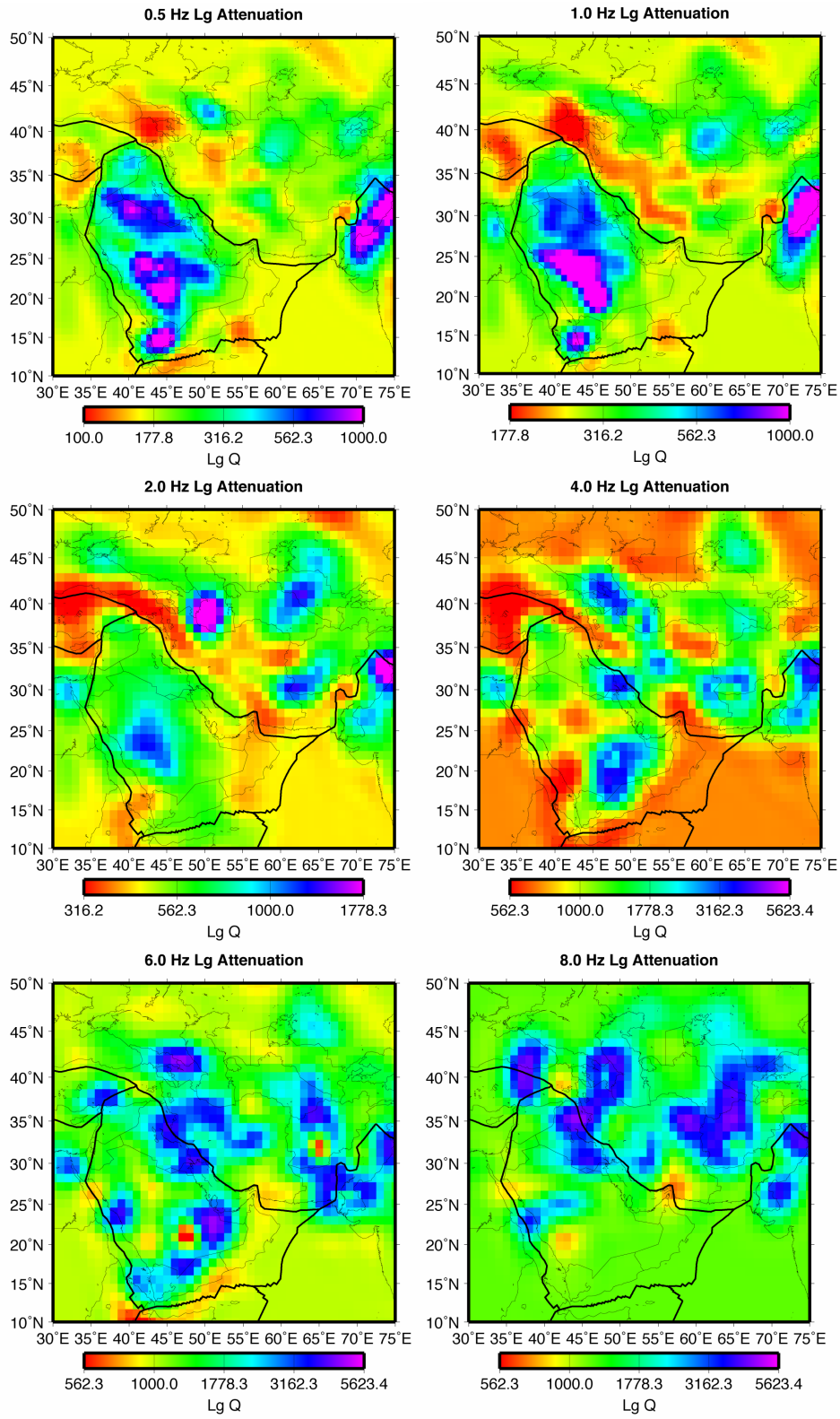
0.5 Hz Lg Attenuation
1.0 Hz Lg Attenuation
2.0 Hz Lg Attenuation
4.0 Hz Lg Attenuation
6.0 Hz Lg Attenuation
8.0 Hz Lg Attenuation
50°N
45°N
40°N
35°N
30°N
25°N
20°N
15°N
10°N
30°E 35°E 40°E 45°E 50°E 55°E 60°E 65°E 70°E 75°E
100.0 177.8 316.2 562.3 1000.0
177.8 316.2 562.3 1000.0
316.2 562.3 1000.0 1778.3
562.3 1000.0 1778.3 3162.3 5623.4
562.3 1000.0 1778.3 3162.3 5623.4
Lg Q

Figure 9

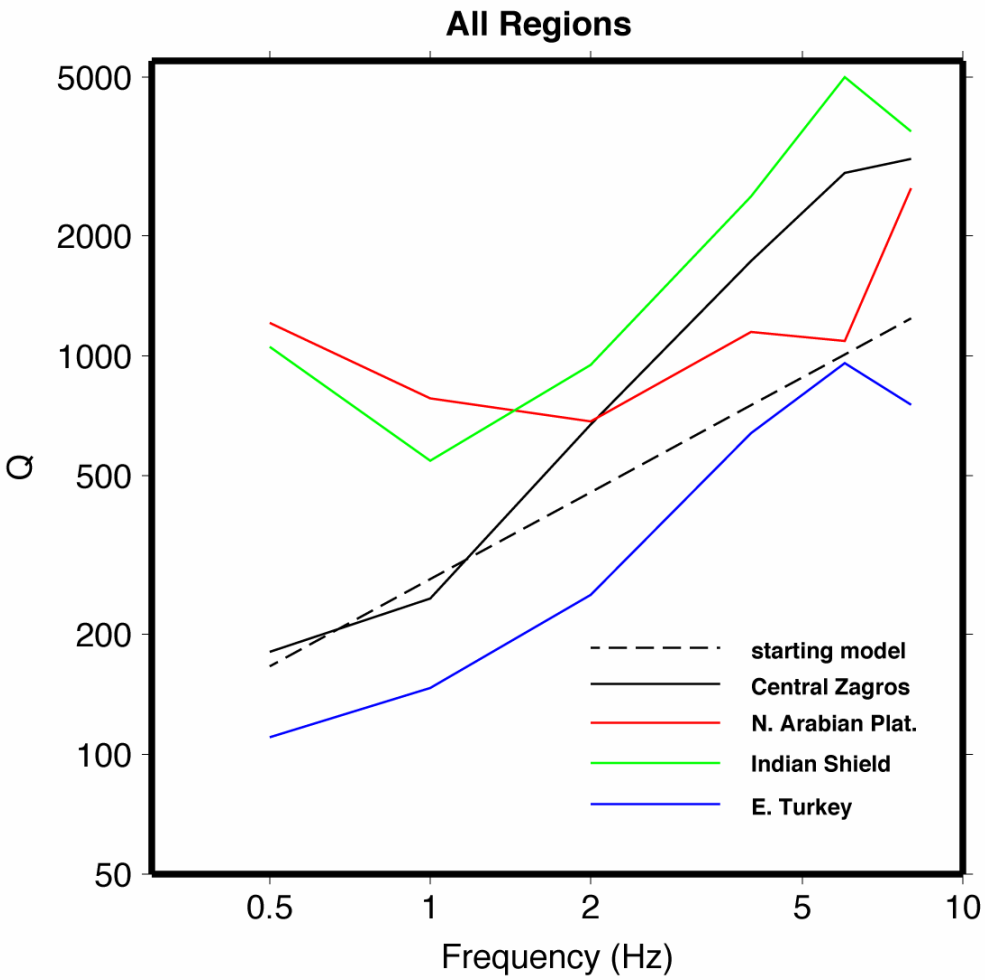
All Regions
5000
2000
1000
500
200
100
50
Q
0.5
1
2
5
10
Frequency (Hz)
starting model
Central Zagros
N. Arabian Plat.
Indian Shield
E. Turkey

Figure 10